Using High-Accuracy Swing Arm Gantry In Spherical Near-Field Automotive Measurement Systems

Vivek Sanandiya, Tim Schwartz, Eric Kim
NSI-MI Technologies
Suwanee, GA 30024 USA
vsanandiya@nsi-mi.com
tschwartz@nsi-mi.com
ekim@nsi-mi.com

***Abstract*—Spherical Near-Field (SNF) systems using a swing arm gantry configuration have been the "go to" solution for automotive measurement systems. Recent advances in the automotive industry have warranted a need for SNF systems with high mechanical positioning accuracy supporting measurements up to 40 GHz and beyond. This paper presents the design and implementation of a new swing arm gantry positioner having an 8-meter radius and a radial axis to support high frequency SNF measurements.**

We first define the relation of the gantry axis to the global coordinate system and discuss primary sources of error. Next, a robust mechanical design is presented including design considerations and implementation. We then present errors measured using a tracking laser interferometer for probe position through the range of gantry axis travel. Static corrections for probe positioning errors are implemented in the control system using the radial axis. The resultant residual error for the swing arm gantry is then shown to have the accuracy required for high frequency SNF measurements.

Keywords—spherical near-field, swing arm gantry positioner, automotive measurement

I. INTRODUCTION

High performance SNF vehicle test systems have historically used arch structures with a carriage riding on a curvilinear track for theta axis motion of the probe. With this arrangement, the probe aperture location at each theta axis position can be fine-tuned through adjustment of the track system until the desired probe alignment accuracy is achieved. A downside to this type of architecture is a permanently mounted structure weighing many thousands of pounds for systems designed for all but the smallest of test articles. The presence of the structure also limits the possibility of other types of measurements in the chamber. An alternate arrangement, using a rotating gantry arm for theta axis motion, has been used before, but with limited fidelity and frequency range due to deflections inherent in the gantry arm. These limitations can be overcome though careful design and the use of error correction to compensate for the nonlinear gravitational deflections. Also, by mounting the gantry arm on a vertical slide assembly, the gantry arm can be stowed below floor level, allowing for other types of measurements within the same chamber.

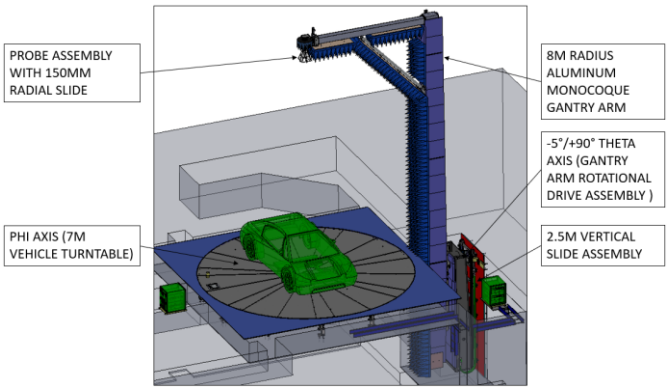

Figure 1. SNF Sytem with Swing Arm Gantry

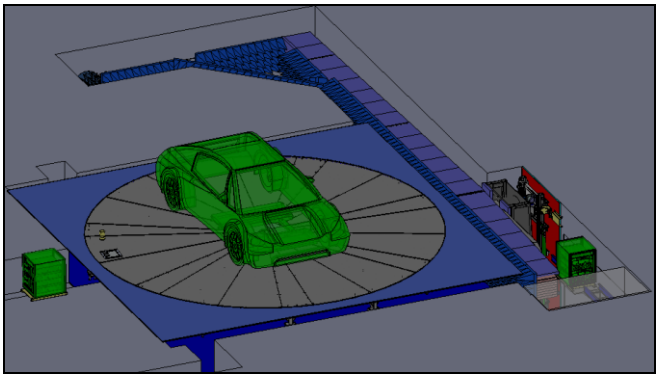

Figure 2. SNF with Gantry in Stowed Configuration

The system shown in Figure 1. is an example of this architecture that was recently installed and incorporates a 7 m diameter vehicle turntable with an 8 m radius gantry arm. The gantry arm is mounted on a vertical lift with a 3 m total travel range, which allows the center of the measurement sphere to be positioned from 0-2.5 m above the turntable surface. The probe is mounted on a 150 mm, high precision radial slide atop the gantry arm. This radial slide allows the radius of the probe aperture to be corrected as a function of the theta axis position. The theta axis position is also corrected as a function of its own position. These two error corrections are carried out in the position controller through application of error maps created from data gathered with a tracking laser. The commanded positions of the theta and radial axes incorporate these

corrections and result in actual probe aperture position errors that are comparable to those of arch based measurement systems.

II. Mechanical Design and Analysis

A. *Swing Arm Gantry Design*

The gantry arm uses an aluminum monocoque design to maximize the stiffness to weight ratio, thereby minimizing deflection of the probe aperture throughout its travel range. A multi-piece design was utilized due to limitations on readily available material stock sizes that would have been required for a single piece 8 m monocoque structure. The multi-piece design allows for an optimized wall thickness for each section, with lower sections having increasing wall thicknesses to better withstand the higher bending stresses. Composite fabrication could also be utilized, but the desired performance was achieved at a significantly lower cost with the presented aluminum design. A thin wall aluminum support strut is integrated to minimize vertical deflections at the 0° theta position, the most critical measurement location in an SNF measurement. The gantry arm incorporates an adjustable counterweight to locate the center-of-gravity (CG) of the rotating mass as close as possible to the theta axis of rotation. By doing this, deflections of the vertical slide assembly remain consistent regardless of the theta axis position. The vertical slide carriage frame & rail system components are fabricated from steel and use high capacity linear bearings to minimize deflection as the gantry rotation axis is positioned to the desired measurement height. The vertical slide actuator also features a self-locking acme screw and fail-safe motor brake to ensure safety from unintended lowering of the arm in the event of a power outage. All axes of motion utilize low-backlash drivetrains and encoder position feedback to control any unwanted motion of the probe.

B. *Finite Element Analysis (FEA)*

FEA was used for preliminary estimation of the nonlinear probe aperture deflection errors. Vertical deflections of the probe can be compensated for with the axes present in the system shown in Figure 1. . The largest probe aperture errors occur at the theta axis positions of 0° and 90°. At 0°, the probe aperture downward deflection results in the largest radial position error, with an estimate of -0.19” (-4.8 mm) from FEA. This error decreases in magnitude as the theta axis rotates towards its forward travel limit at +90°. These radial errors are corrected through proportional radial slide adjustments as a function of the theta axis position.

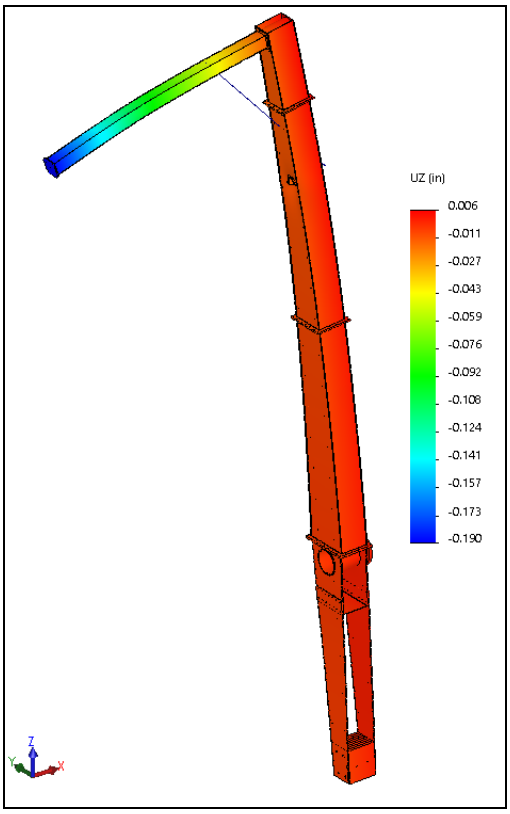

Figure 3. 8 m Gantry Arm Finite Element Analysis Vertical Deflection (0° Theta)

At 90°, the probe aperture downward deflection estimate from FEA was -1.064” (-27.0 mm). This results in the largest theta axis angular error that equates to an angular deflection of:

$$\alpha = \text{atan}\,(27/8000) = 0.194\text{deg} \qquad (1)$$

This deflection error type decreases in magnitude as the theta axis position gets closer to 0° and is corrected through a proportional offset to the theta axis commanded position.

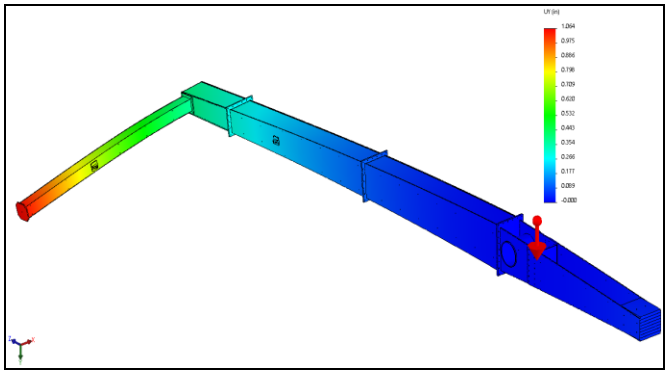

Figure 4. 8m Gantry Arm Finite Element Analysis Vertical Deflection (90° Theta)

III. GLOBAL POSITIONING ERRORS

The overall accuracy of an SNF measurement system is affected by several geometric errors. The analysis and effects of these errors is beyond the scope of this paper and can be found in [1] and [2].

In this section, we discuss the dominant global positioning error terms due to deflection in a swing arm gantry and show uncorrected positioning error measured using a laser interferometer.

A. Global Positioning Errors

The following dominant errors can be defined as shown in Figure 5. and Figure 6.

1) Theta-Zero Error: The depointing of probe relative to Z-axis in X-Z plane when position controller indicates Theta = 0deg.

2) Theta Positioning Error: Error in theta due to sag in the gantry arm.

3) Radial Error: The deviation in measurement radius as function of theta.

4) Lateral Error: Out of plane translation of probe as it moves in theta.

5) Non-Orthogonality Error: Non orthogonality between the theta and phi axes.

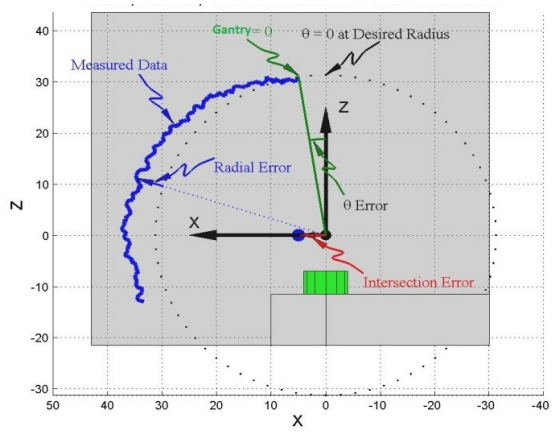

Figure 5. Theta and Radial Error Illustration

The lateral and non-orthogonality errors present due to the probe aperture moving out of plane as it's swept over the theta axis travel range would normally require a cross-range slide that was not present in the system being presented. In practice, these deflections proved to be easily compensated for by adjustment of the vertical slide assembly's alignment relative to gravity.

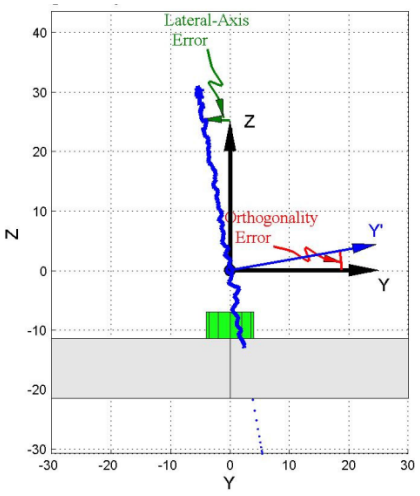

Figure 6. Lateral Error Illustration

B. Uncorrected Error Measurements

A laser interferometer is used to establish the coordinate system and measure theta positioning error and radial error. position of the probe aperture is measured as it moves in theta using a probe simulator [3] to determine theta positioning error and radial error.

Figure 7. shows the error in theta due to the sag in gantry arm. Note the max error is at theta = 90°, the measured error of 0.214° is consistent with the FEA analysis result of 0.194°. The small difference is within margin of analysis and could be due to the variation in weight of absorber and probe in the system vs. the model.

Figure 7. Theta Error vs. Theta

Figure 8. shows the radial error as the gantry moves in theta due to the sag in gantry. This error is maximum at theta = 0°. The measured error of 0.19" shows good agreement with the FEA analysis result.

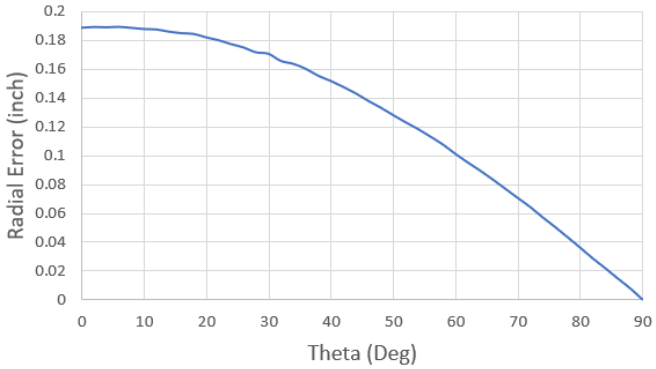

Figure 8. Radial Error vs. Theta

The error curves shown in Figure 7 and 8 display sinusoidal and cosinusoidal behavior as expected and also observed in [4] for a smaller mm-wave SNF swing-arm scanner.

IV. Error Correction using the Position Controller

In this section we discuss the error maps, implementation of error correction, and the residual error.

A. Construction of Error Maps

The measured position error can be represented using simple equations to facilitate implementation of error correction. The sinusoidal and cosinusoidal nature of the errors can be used to formulate error correction terms as shown here.

For the error in theta, the measured error can be represented by following equation,

$$\theta_c = \theta_0 + A*\text{Cos}(\theta) + B*\text{Sin}(\theta) \quad (2)$$

Where, θ_c = Theta Error Correction Factor

θ_0 = Theta-Zero Offset

θ = Commanded Theta

A & B are correction coefficients

Figure 9. shows the correction term and measured theta error with $\theta_0 = 0$, A = 0.2142, and B = 0.

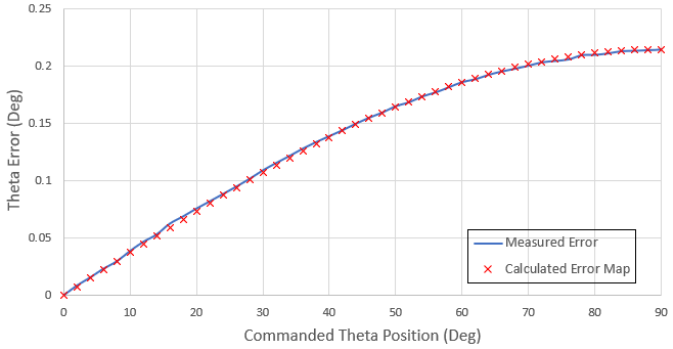

Figure 9. Theta Error and Correction Factor vs. Theta

Similarly, the radial error can be represented by the following equation,

$$R_c = R_0 + C*\text{Cos}(\theta_c) + D*\text{Sin}(\theta_c) \quad (3)$$

Where, R_c = Radial Error Correction Factor

R_0 = Radial Offset

C & D are correction coefficients

Figure 10. shows the correction term and measured theta error with $R_0 = -0.012$, C = 0.202, and D = 0.0133.

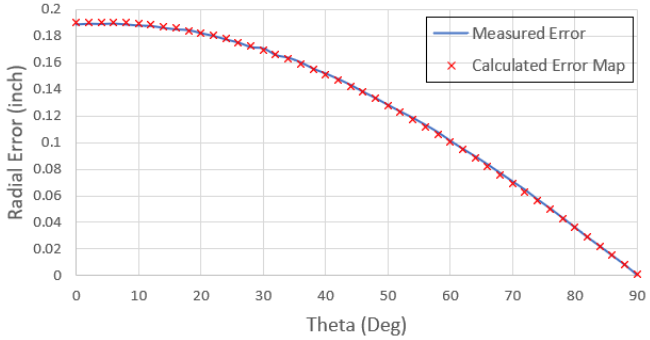

Figure 10. Radial Error and Correction Factor vs. Theta

B. Error Correction Implementation

The error map can be stored in the form of an equation or a lookup table in the NSI-MI ELE-IPC position controller. A script that uses built-in controls from the ELE-IPC controls the error correction.

The ELE-IPC position controller actively performs error correction as follows:

- The ELE-IPC provides the control of motion for the theta and radial axes of the gantry.
- The error map in the form of an equation or lookup table is loaded into the controller.
- The controller implements error correction using its coordinated motion feature on the theta and radial axes as the theta axis is moved or stepped.

The ELE-IPC implements coordinated motion using Lua scripts that are created using the NSI-MI 3001 workstation and downloaded to the controller. These scripts combine one or more axes that are under the control of the ELE-IPC into a "virtual axis" that can be controlled as a single entity. As the virtual axis moves, functions in the scripts are called for each of the constituent axes to provide motion information for each axis.

To make use of error maps in this system, we constructed a virtual axis theta with physical theta and radial axes. A "move" command to the virtual theta axis triggers the calculation or lookup of the theta and radial errors, the ELE-IPC then commands motion of the theta and radial axes to the position returned by the equation or lookup table. The move is complete when the physical axes are at their corrected positions. This

process is repeated each time the virtual theta axis is commanded to move.

C. *Residual Error After Correction*

The residual theta and radial errors are shown in Figure 11. and Figure 12. after error correction. Theta error limits of +/-0.0035° and radial error limits of +/-0.0015" (+/-0.0381mm) were achieved. The radial error level corresponds to less than λ/100 at 40GHz, demonstrating the capability of using the gantry design for SNF measurements up to 40GHz and beyond. While the uncorrected positional errors in a gantry are significantly higher compared to an arch, the residual post-correction errors show comparable performance to high accuracy arches shown in [5-7].

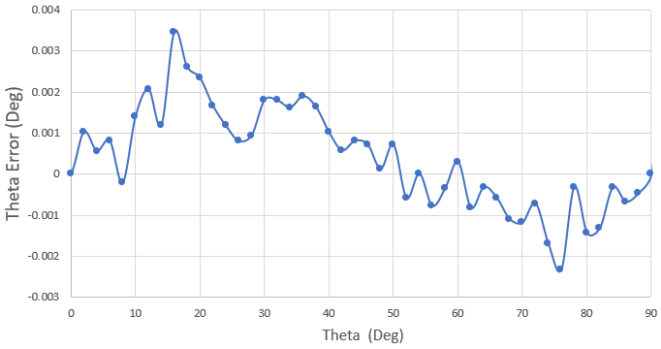

Figure 11. Residual Theta Error vs. Theta

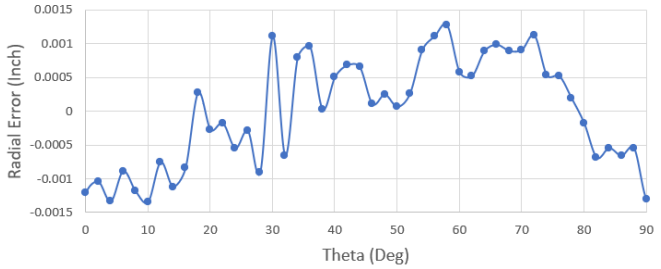

Figure 12. Residual Radial Error vs. Theta

The residual errors remaining after correction approach the inherent accuracy of the physical axes used for the correction.

V. CONCLUSION

A high accuracy spherical near-field gantry has been designed and constructed to enable characterization of automotive test articles with demanding requirements. Position correction was incorporated to correct residual errors in the theta angle and radius of the measurement system as a function of theta using the coordinated motion capabilities of the NSI-MI ELE-IPC position controller.

The presented data demonstrate that the residual error magnitudes can be greatly reduced using the error correction system. The levels of accuracy achieved set a new standard for large Swing Arm Gantries used in SNF automotive measurement systems.

REFERENCES

[1] Hansen, J.E., Spherical Near-Field Antenna Measurements. Peter Peregrinus Ltd., 1988.

[2] Hess, Doren W., "An Expanded Approch to Spherical Near-Field Uncertainity Analysis," Antenna Measurement Techniques Association 24th Annual Meeting & Symposium (AMTA-02), Cleveland, OH, pp 495-500

[3] Pierce, S. and Langston, J., "Implementation of a Geometric-Error Correction System for Extremely High Probe Position Accuracy in Sperical Near-Field Scanning", AMTA Meeting & Symposium, pp. 93-97, Atlanta, GA, 2004.

[4] Clive Parini, Stuart Gregson, John McCormick, Daniel Janse van Rensburg, "Theory and Practice of Modern Antenna Range Measurements", IET Publications, 2007, pp. 404-409

[5] J. Fordham, T. Schwartz, G. Cawthon, Y Netzov, S. McBride, M Awadalla, . D. Wayne, "Achieved accuracy of a spherical near-field arch positioning system", European Conference on Antennas and Propagation (EUCAP), pp. 3195- 3199, 2012.

[6] McBride, S., Marier, J., Kryzak, C., Fordham, J. and Liu, K., "A Large Spherical Near-Field Arch Scanner for Characterizing Low-Frequency Phased Arrays", AMTA Proceedings, pp. 71-76, Atlanta, GA, 2010.

[7] Pierce, S., Liang, C.., "Alignment of a Large Spherical Near-Field Scanner Using a Tracking Laser Interferometer", AMTA Proceedings, pp. 64-69, Irvine, CA, 2003.